JCTC Journal of Chemical Theory and Computation

Article

pubs.acs.org/JCTC

CH Stretching Region: Computational Modeling of Vibrational Optical Activity

Jana Hudecová,[†,§] Václav Profant,[†] Pavlína Novotná,[‡] Vladimír Baumruk,[†] Marie Urbanová,[‡] and Petr Bouř*[,§]

[†]Faculty of Mathematics and Physics, Institute of Physics, Charles University, Ke Karlovu 5, 12116, Prague 2, Czech Republic

[‡]Department of Physics and Measurements and Department of Analytical Chemistry, Institute of Chemical Technology, Technická 5, 16628 Prague, Czech Republic

[§]Institute of Organic Chemistry and Biochemistry, Academy of Sciences, Flemingovo náměstí 2, 16610 Prague, Czech Republic

Supporting Information

ABSTRACT: Most organic compounds provide vibrational spectra within the CH stretching region, yet the signal is difficult to interpret because of multiple difficulties in experiment and modeling. To better understand various factors involved, the ability of several harmonic and anharmonic computational approaches to describe these vibrations was explored for α-pinene, fenchone, and camphor as test compounds. Raman, Raman optical activity (ROA), infrared absorption (IR), and vibrational circular dichroism (VCD) spectra were measured and compared to quantum chemical computations. Surprisingly, the harmonic vibrational approach reasonably well reproduced the measured spectral patterns, including the vibrational optical activity (VOA). The CH stretching, however, appeared to be more sensitive to the basis set and solvent variations than lower-frequency vibrations. For a higher accuracy in frequencies and spectral shapes, anharmonic corrections were necessary. Accurate harmonic and anharmonic force fields were obtained with the mPW2PLYP double-hybrid functional. A limited vibrational configuration interaction (LVCI) where the CH stretching motion was decoupled from other vibrations provided the best simulated spectra. A balanced harmonic oscillator basis set had to be used, containing also states indirectly interacting with fundamental vibrations. A simpler second-order perturbational approach (PT2) appeared less useful. The modeling provided unprecedented agreement with experimental vibrational frequencies; spectral shapes were reproduced less faithfully. The possibility of ab initio interpretation of the CH spectral region for relatively large molecules further broadens the application span of vibrational spectroscopy.

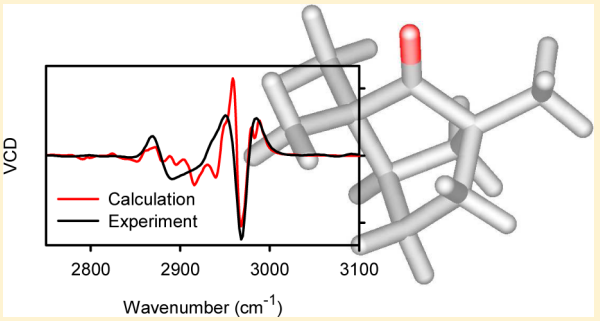

INTRODUCTION

The CH stretching region is traditionally considered as a range of wavenumbers approximately within 2500−3400 cm^{-1} comprising mostly fundamental transitions of the CH valence vibrational motions. Unlike NH, OH or SH stretching vibrations also present in this interval, CH stretching bands are not prone to broadening by hydrogen bonding. Because of the high relative strength of the CH bond and small hydrogen mass, fundamental CH stretching energies are well-separated from other molecular vibrations and can be easily identified in the spectra. They provide rich information not only about molecular stereochemistry[1,2] but also about intermolecular interaction[3] as the hydrogen atoms form large parts of molecular surfaces. For a deuterated system containing the CD bonds (vibrating lower than CH, around 2200 cm^{-1}) even a solute−solvent chirality induction was observed lately.[4] Near-infrared vibrational circular dichroism was proposed for online monitoring of a chemical reaction.[5]

On the other hand, the bond strengths of different CH groups in a molecule are quite similar, which causes overlapping of vibrational bands, and makes the interpretation difficult. Measurements in the CH stretching region are often connected with unusual spectrometer setups. For example, although particularly useful stereochemical information can be obtained from the vibrational optical activity (VOA),[6−8] the CH stretching signal may be weak and prone to artifacts.[9−11]

The potential energy surface governing the hydrogen stretching motion is strongly anharmonic. CH bonds and the coupling terms between them cannot be simply described by quadratic force constants. This often prevents reliable simulation and consequent interpretation of experimental data.[10,12−18] In the past, for example, simpler models or empirical rules were proposed for VOA simulations in this region.[9,19] Some spectral shapes could be reasonably well modeled at the harmonic level, which, however, led to huge frequency errors.[10,20] Obviously, the lower-frequency (around 1400 cm^{-1}) vibrations also profit from an eventual anharmonic correction.[20] So far, in spite of

Received: April 6, 2013

   dx.doi.org/10.1021/ct400285n | J. Chem. Theory Comput. XXXX, XXX, XXX−XXX

considerable progress in computational methodology,[15,21−24] simulations of the CH stretching properties are in general considered to be unreliable.

A significant progress was achieved lately by incorporating the solvent environment to the density functional theory (DFT) simulations of vibrational circular dichroism (VCD).[20,25,26] Even then the anharmonic corrections, although helpful for energies, did not lead to a general improvement in spectral shapes.[26] A mixed message about the performance of the harmonic approximation has thus been obtained in the past. As shown below, some of the confusion can be explained by the stability of the harmonic pattern even when hundreds of thousands of harmonic oscillator (HO) states are allowed to interact within the anharmonic scheme. As shown below, however, these states have to be chosen in a balanced way. This study also suggests that the perturbational approach (PT2) used previously[26] may not be sufficient to treat the anharmonicities, especially for the vibrational optical activity, and should be replaced by the more universal vibrational configuration interaction.

In the first part of this paper, we systematically investigate various factors influencing the quality of both the harmonic and anharmonic computed force fields with respect to the CH stretching behavior. It turns out, for example, that the CH stretching motion is very sensitive to the choice of the basis set and electronic computational level used. Unlike in previous studies, the "complete set" of IR, Raman, Raman optical activity (ROA), and VCD is simulated and compared to experiment to avoid accidental agreement/disagreement of the spectra. In particular, the vibrational optical activity (VCD, ROA) is very sensitive to variations of computational parameters,[27] structure, and molecular force field. For ROA, high-quality experimental spectra in the CH stretching region could be measured, owing to a spectrometer expansion by three grating systems, correction of the intensities against a fluorescence standard, and a careful baseline subtraction. Original VCD spectra were acquired as well, on a spectrometer dedicated to this region.

For the anharmonic computations, we obtained the best results using the limited vibrational configuration method (LVCI) and a limited coupling between the lower- and higher-frequency motions. A faster degeneracy-corrected second order perturbation (PT2)[15] method lead to improvement in frequencies only, without credible intensity reproduction. The LVCI procedure and the limited coupling have been suggested in many variants previously.[12,21,23,28] Our implementation[15,29] allows for a fast diagonalization of a very large vibrational Hamiltonian matrix (~10^6 of HO basis states) and a consistent spectra generation in a "double-anharmonic" approximation where the energy and intensity tensor derivatives are evaluated up to the fourth and second order, respectively.

It is also important to note that the agreement between the computation and experiment would not be possible without the latest availability of the double-hybrid density functionals[30] combining the MP2[31] method with DFT.[32] For relatively large molecules, we are thus getting so far the most balanced converged simulated spectral shapes that considerably improve the harmonic procedure if compared to experiment. Obviously, some discrepancies remain, and we see this study as a step toward full understanding of the molecular vibrational behavior.

METHODS

Spectra Measurement. Raman and ROA incident circular polarized light (ICP) spectra of neat α-pinene, neat fenchone, and 0.2 M CCl_4 solution camphor were acquired on a spectrometer[33] built at the Charles University, Prague. It is based on the 514.5 nm laser excitation wavelength. Owing to three interchangeable gratings and intensity correction using a fluorescence standard (National Institute of Standards and Technology, USA), a wide wavenumber range (~50 ... 3400 cm^{-1}) became accessible. The laser power was set to 500 mW, the total acquisition time was about 20 h for each sample and grating, and the measurements were performed using low-volume quartz cells with antireflectively coated windows. Raw ROA spectra were filtered by Fourier transform to suppress quasiperiodic high-frequency CCD signal. For camphor, the solvent (CCl_4) signal was subtracted. For Raman spectra, the empty cell signal was subtracted and the baseline was slightly straightened by a polynomial fit. ROA artifacts were eliminated by measuring and averaging both enantiomers without further correction. The measurement of both enantiomers was particularly important for the CH stretching signal, where the circular intensity difference[34] (CID) ratio of the ROA and Raman signals is as small as ~5×10^{-5}. Spectra of the (1*R*)-(+)-α-pinene, (1*R*)-(−)-fenchone, and (1*R*)-(+)-camphor enantiomers (Figure 1) are presented.

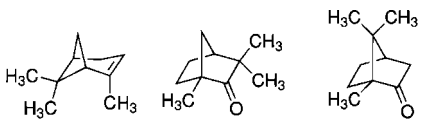

α-pinene fenchone camphor

Figure 1. Studied molecules: (1*R*)-(+)-α-pinene (2,6,6-trimethylbicyclo[3.1.1]hept-2-ene), (1*R*)-(−)-fenchone (1,3,3-trimethylbicyclo[2.2.1]heptan-2-one), and (1*R*)-(+)-camphor (1,7,7-trimethylbicyclo [2.2.1]heptan-2-one).

VCD and IR spectra were measured on a FTIR IFS 66/S spectrometer equipped with a PMA 37 VCD/IRRAS module (Bruker, Germany). The samples were placed in a demountable cell (A145, Bruker, Germany) composed of KBr and CaF_2 windows separated by a 6, 50, or 100 μm Teflon spacer with a spectral resolution of 4 or 8 cm^{-1}, and averages of 6−16 blocks of 3686 scans were used. The spectra were corrected for the baseline and artifacts as for ROA. The experimental conditions for all compounds and spectral ranges are summarized in Supporting Information Table S1.

Electronic and Harmonic Vibrational Computations. α-Pinene, fenchone, and camphor geometries were optimized by energy minimization using the Gaussian09 program.[35] The Raman, ROA, IR, and VCD spectra were calculated at the same level within the harmonic approximation also by Gaussian. Various quantum chemical models and functionals (HF, MP2,[31] B2PLYP, B3LYP, BPW91, B3PW91,[36] CAM-B3LYP,[37] mPW2PLYP,[30] and dispersion-corrected[30,38] mPW2PLYP = "mPW2PLYP-D") and basis sets (6-31G, D95, 6-31G*, TZV, 6-31+G*, 6-31G**, D95**, TZVP, 6-31++G**, D95++**, 6-311++G**, cc-pVTZ, and aug-cc-pVTZ) were combined in order to investigate the behavior of the CH stretching vibrations. Computation of the ROA intensity tensors is not implemented within mPW2PLYP; thus they were calculated at the DFT B3LYP/6-311++G**/COSMO level. Previous experience suggests that the error associated with such simplification would be very small.[39−41]

The molecular environment was accounted for by the COSMO[42] dielectric model. For a deeper insight, nine different

dx.doi.org/10.1021/ct400285n | J. Chem. Theory Comput. XXXX, XXX, XXX−XXX

solvents of a broad scale of relative dielectric constants (ε_r, given in parentheses, see also Supporting Information Table S2) were used for camphor (vacuum (1), argon (1.43), carbon tetrachloride (2.23), chloroform (4.71), dichloromethane (8.93), 2-hexanone (14.14), methanol (32.61), water (78.36), and formamide (108.94)). The experimental conditions were mimicked by $\varepsilon_r = 2.23$ (camphor solution in carbon tetrachloride), $\varepsilon_r = 2.69$ (neat α-pinene, using Gaussian parameters for pentanoic acid), and $\varepsilon_r = 12.51$ (neat fenchone, using Gaussian parameters for 1-hexanol). A spherical polarization factor[43] defined as $\eta = (\varepsilon_r - 1)/(2\varepsilon_r + 1)$ was conveniently used as the principal solvent characteristic, as many spectroscopic properties are approximately linear in η. All theoretical spectral profiles were generated by a convolution of calculated intensities with a Lorentzian function 10 cm^{-1} wide (full width at half-maximum). Incident circular polarized (ICP) Raman and ROA spectral profiles were adjusted by a Boltzmann factor[44] to 298 K and expressed as intensity sums ($I^R + I^L$, Raman) and differences ($I^R - I^L$, ROA) for the right- and left-circular polarized lights. Note that in experiment absolute Raman and ROA intensities are not measured; therefore, the computed and experimental intensities were scaled to have similar magnitudes. The IR absorption (ε) and VCD ($\Delta\varepsilon$) spectra are expressed in the standard units of $L\cdot cm^{-1}\cdot mol^{-1}$. No scaling was applied to computed frequencies.

Anharmonic Corrections. We used a limited Taylor expansion of the vibrational potential, where the anharmonic part is given by

$$W(Q_1, \ldots, Q_M) = \frac{1}{6}\sum_{i=1}^{M}\sum_{j=1}^{M}\sum_{k=1}^{M} c_{ijk}Q_iQ_jQ_k + \frac{1}{24}\sum_{i=1}^{M}\sum_{j=1}^{M}\sum_{k=1}^{M}\sum_{l=1}^{M} d_{ijkl}Q_iQ_jQ_kQ_l \quad (1)$$

where Q_i are the normal mode coordinates, c_{ijk} and d_{ijkl} are the cubic and quartic constants. All cubic and semidiagonal ("$iijk$", etc.) quartic constants were obtained by two-step differentiation of the second energy derivatives. The differentiation was performed in dimensionless[45] normal mode coordinates q_i, with a step of $\Delta q_i = \Delta Q_i \times 1000/\omega_i$, where $\Delta Q_i = 0.05$ atomic units, and the harmonic frequency ω_i is in inverse centimeters. The variable step size prevents too small displacements for the lowest-frequency modes.[46]

The PT2 and LVCI schemes were used for anharmonic corrections to vibrational energies and spectral intensities. Within PT2, the harmonic vibrational energy for each state n, E_n, is corrected by $E_n^{(1)} = W_{nn}$ and by a second-order term,

$$E_n^{(2)} = \sum_{m\neq n} A_{mn} \quad (2)$$

where $A_{mn} = [E_m - E_m \pm ((E_m - E_m)^2 + 4W_{mn}{}^2)^{1/2}]/2$, the plus sign holds for $E_n > E_m$ and minus sign for $E_n < E_m$, and $W_{nm} = \langle n|W|m\rangle$ Similarly, the PT2 wave function was considered as $\psi_n' = \psi_n - \sum_{m\neq n} A_{mn}W_{mn}{}^{-1}\psi_m$, ψ_n is the unperturbed state.

The spectral properties were considered to be dependent on the coordinates to second order as

$$P = P_0 + \sum_i P_{1,i}Q_i + \frac{1}{2}\sum_{i,j} P_{2,ij}Q_iQ_j \quad (3)$$

where P is the electric dipole moment (for IR) or the polarizabilities ($\boldsymbol{\alpha}$, $\mathbf{G}'$, $\mathbf{A}$, for Raman and ROA intensities). For VCD, we also used the dependence of the magnetic dipole moment on the coordinates and momenta Π_i.

$$m = m_0 + \sum_i A_{1,i}\Pi_i + \frac{1}{2}\sum_{i,j} A_{2,ij}(\Pi_iQ_j + Q_j\Pi_i) \quad (4)$$

$A_{1,i}$ is the axial tensor. Note that within the magnetic field perturbation theory, the magnetic derivatives can be treated in the same way as for the coordinate derivatives, i.e. within the Born–Oppenheimer approximation.[47]

Transitional PT2 dipole moments and polarizabilities[34,48] were obtained as $\langle i'|P|0'\rangle/(N_iN_0)^{1/2}$ (for a transition $\psi_0' \rightarrow \psi_i'$), with renormalization factors $N_i = 1 + \sum_{j\neq i}|\langle i|W|j\rangle|^2E_{ij}^{-2}$, $E_{ij} = E_i - E_j$.

In LVCI, vibrational wave function was expanded to the HO wave functions, $\Phi_\varepsilon = \sum_f C_f^\varepsilon\psi_f$. As in previous studies,[15,21] several criteria were employed to limit the number of HO basis functions. The lowest-frequency normal modes (e.g., up to mode number 36) were not excited, and only states (f) obliging $W_{fn} > c_1|E_n - E_f|$ were included, where c_1 is an interaction parameter and n is a ground or fundamental state. A second set of HO basis functions (f') was added based on coefficient c_2, interacting with the already chosen basis ($W_{f'f} > c_2|E_{f'} - E_f|$). Hamiltonian elements with too energy-separated states ($|H_{ij}| < 10^{-4}|E_i - E_j|$) were excluded as well.

Up to five-times excited wave functions were used, and the coefficients C_f^ε and associated energies E_ε were obtained from the Hamiltonian matrix by Mitin's version[49] of the Davidson[50] diagonalization procedure. Previously, a Fourier transform (FT) based procedure for large matrix diagonalization was also proposed for generation of anharmonic molecular spectra.[29] In this study, we prefer the Davidson approach because it provides exact eigenstates without the need to calibrate the FT convergence,[29] and allows us to include anharmonic (second-order) derivatives of the intensity tensors.

Diagonalization Algorithm. For LVCI, the large Hamiltonian diagonalization is of central importance for the spectra generation. We provide a brief description of the algorithm:

(1) Select the HO states $\{\psi_n\}$ based on the restrictions above and calculate elements of the vibrational Hamiltonian H_{ij}. Save indices and values for the large elements only.
(2) Load them in memory (e.g., in an array **a**, for each row i recorded in a_{ms} ... a_{ms+ni}, keep a number of these elements n_i, starting index m_s, and the column index in an array **j**).
(3) To solve the eigenvalue problem, $\mathbf{H}\cdot\mathbf{c}^\lambda = E_\lambda\mathbf{c}^\lambda$, set $\lambda = 0$ and $M = M_{max} = 10$. Set **d** to a unit vector and $E_d = 0$.
(4) Increment λ by 1. For $\lambda > 1$, set $\mathbf{d} = \sum_{J=1}^{M} w_J{}^2\mathbf{X}_J$ and $E_d = z_2$.
(5) Set $\mathbf{c}^\lambda = \mathbf{d}$ and $E_\lambda = E_d$. Orthogonalize $\mathbf{c}^\lambda$ to vectors $\{\mathbf{c}^\mu\}_{\mu=1\ldots\lambda-1}$ and normalize so that $|\mathbf{c}^\lambda| = 1$.
(6) Construct "gradient vectors"[49] $\{\mathbf{x}_J\}_{J=1\ldots M}$ as $\mathbf{x}_1 = \mathbf{c}^\lambda$ or $\mathbf{x}_J = \mathbf{H}\cdot\mathbf{x}_{J-1} - E_\lambda\mathbf{x}_{J-1}$ (for $J > 1$), orthonormalize each against the previous gradient vectors $\{\mathbf{x}_K\}_{K=1\ldots J-1}$ and eigenvectors $\{\mathbf{c}^\mu\}_{\mu=1\ldots\lambda-1}$. If $|\mathbf{x}_2| <$ tolerance, record E^λ and $\mathbf{c}^\lambda$; if also $E^\lambda < E_{lim}$ ($E_{lim} \sim 2400$ cm^{-1} for $E^1 \sim -800$ cm^{-1}), go to 4; else, stop. Typically, tolerance ~ 1.
(7) Search for a new eigenvector λ as a combination of the gradient vectors, $\mathbf{c}^\lambda = \sum_{J=1}^{M} w_J\mathbf{X}_J$: Construct $A_{IJ} = \mathbf{x}_I\cdot\mathbf{H}\cdot\mathbf{x}_J$ and solve the reduced dimension ($M \times M$) eigenproblem $\mathbf{A}\cdot\mathbf{w}^L = z_L\mathbf{w}^L$.

dx.doi.org/10.1021/ct400285n | J. Chem. Theory Comput. XXXX, XXX, XXX–XXX

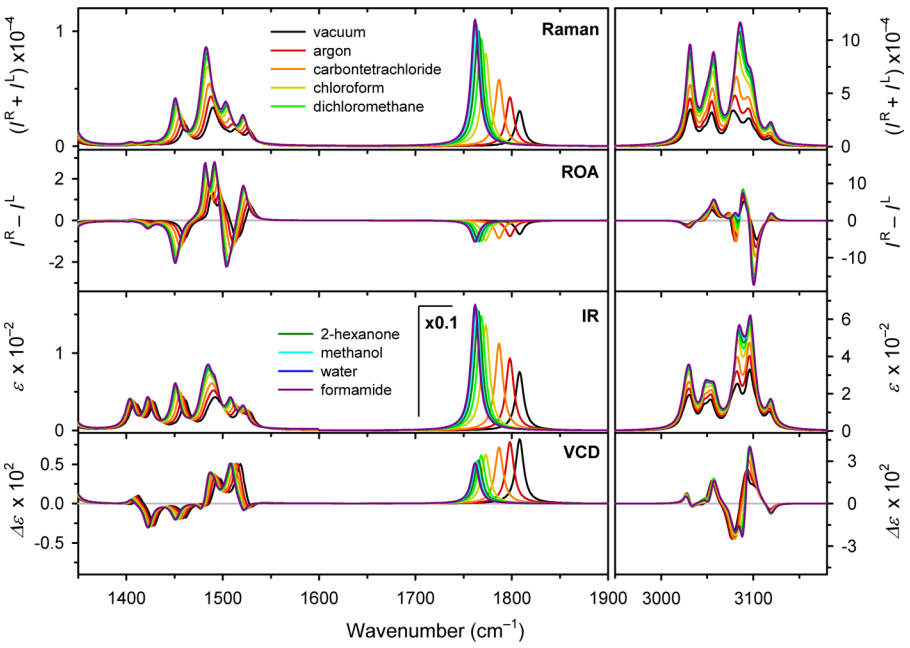

Figure 2. Solvent dependence of the calculated (B3LYP/6-311++G**/COSMO) (1*R*)-(+)-camphor Raman, ROA, IR, and VCD spectra.

(8) Check if the subspace is not redundant: for $K = 4 \ldots M$, if $|\mathbf{w}^K| < 10^{-10}$ reduce M by 1 (if still larger than 3). But if $|\mathbf{w}^M| > 10^{-10}$ and $M < M_{max}$, increase M by 1.

(9) Set $E_d = z_1$ (lowest eigenvalue) and $\mathbf{d} = \sum_{j=1}^{M} w_j^1 \mathbf{x}_j$. Go to 5.

The restriction to the large H_{ij} elements (steps 1 and 2) provided significant memory saving enabling real time computation without a data swapping on the disk. For the dimension of 1 086 008 used in the camphor computation, for example, from the total of 589 707 231 036 elements, 561 913 420 (~0.05%) were selected, requiring about 6.7 GB of memory only. The possibility to keep the Hamiltonian and eigenvectors in memory enables efficient parallelization of the code. As another enhancement, only large eigenvector elements ($|C_i^\lambda| > 10^{-4}$) were kept in memory, which had a negligible effect on the precision but significantly reduced the computational time needed for the multiple vector orthonormalization procedures (steps 5 and 6).

RESULTS AND DISCUSSION

Experimental Spectra. The experimental spectra (Figure S1) of α-pinene, fenchone, and camphor are consistent with previous data.[4,10,20,51−55] The VOA measurements in the high-frequency CH stretching region required special care to minimize artifacts. In particular, the measurement of ROA was difficult because of the low ROA/Raman circular intensity difference (ratio of ROA and Raman intensities, CID)[34] which is given by the relatively large Raman signal of the C−H stretching modes. An example of the artifact removal is shown for α-pinene in Figure S2. The problems of the artifacts in ROA measurement are discussed in detail in ref 56. Currently, both enantiomers have to be available for acquiring reliable ROA spectra in the CH stretching region, some of which could also be verified by comparison with previous measurements.[51,56]

Solvent Dependence of Spectral Intensities. The dependence of the spectra on the solvent environment in the computations has often been neglected in the past, which can lead to very poor agreement to experiment. For example, only about 25% of average spectral VCD intensities could be reproduced by vacuum computation on terpenes.[53] It is generally believed that the interaction of the aliphatic CH group with a solvent is limited; this is, however, not true in terms of the absolute spectral intensities. We choose camphor for the solvent testing as this molecule is normally in a solid state and it is usually dissolved for VOA measurement.

As can be seen in Figure 2, although stretching frequencies do not significantly change under solvent variations, the intensities vary for all the Raman, ROA, IR, and VCD spectral types in the CH region at least to the same extent as for other vibrations. Already the argon environment causes a notable (~10−20%) increase of the intensities. The increase approximately saturates for solvents more polar than 2-hexanone, where the calculated Raman/ROA and IR/VCD intensities are respectively about four and two times larger than in vacuum. Relative CID ratios for different vibrational bands are also varying with solvent polarity. On average, however, CID magnitudes remain rather constant throughout the entire spectral region. The fact that the magnitudes of the Raman and ROA spectra, for example, react to the environment in the same way thus contributed to previous successes of the vacuum-based VOA modeling.[57,58]

The dependence of integral Raman and IR intensities on the solvent polarity plotted in Figure 3 (upper two panels) reveals that the CH stretching vibration are significantly more influenced than the rest, except for the carbonyl stretching. In Figure 3 (bottom), we also compare the dependencies of the isotropic electric dipole polarizability ($\boldsymbol{\alpha}$), dipole moment, and the magnetic ($\mathbf{G}'$) and quadrupole ($\mathbf{A}$) polarizabilities[34] on the polarization factor η. As expected, the dependencies are about linear. The $\mathbf{G}'$ tensor is the least and $\mathbf{A}$ is the most sensitive to the polarity. Therefore, the similar increase in magnitudes of the Raman (dependent on derivatives of $\boldsymbol{\alpha}$) and ROA (dependent on $\boldsymbol{\alpha}$, $\mathbf{G}'$, and $\mathbf{A}$ derivatives) intensities with the polarity appears rather accidental, given by the balance of the $\mathbf{G}'$ and $\mathbf{A}$ contributions.

Similar intensity changes as for CH stretching occur in the lower-frequency region below 1900 cm^{-1}, where they are additionally accompanied by notable changes of vibrational frequencies (Figure 3; individual transition frequencies are

dx.doi.org/10.1021/ct400285n | J. Chem. Theory Comput. XXXX, XXX, XXX−XXX

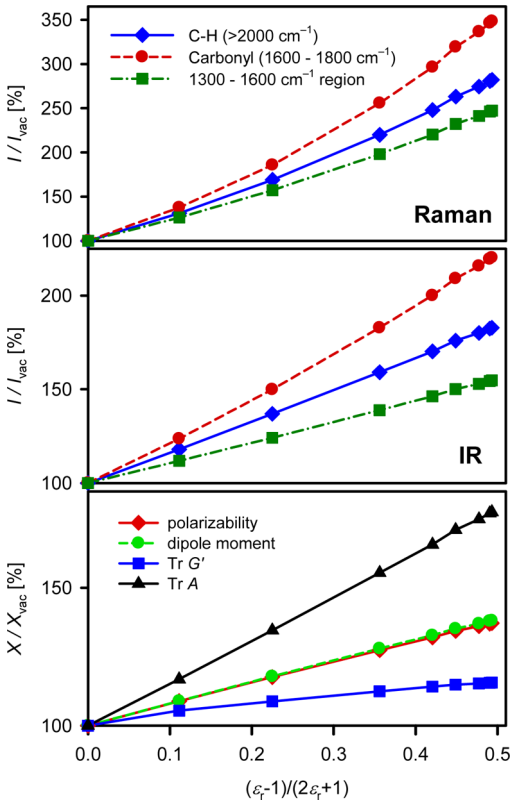

Figure 3. Dependence of calculated integral Raman and IR (1R)-(+)-camphor spectral intensities, dipole moment, and isotropic polarizabilities on the solvent polarization factor, relative to vacuum. For the **A**-tensor, we define Tr $\mathbf{A} \equiv \sum_{\alpha=1..3} A_{\alpha\alpha\alpha}$.

extracted in Supporting Information Figure S3). The C═O stretching band (~1770 cm^{-1}) exhibits the largest shifts, about 50 cm^{-1} for the entire range of solvents. As discussed before,[59−62] even larger shifts can occur experimentally because of the inadequacy of the continuum models for the carbonyl group forming hydrogen bonds. Whereas the increasing solvent polarity causes mostly downshift of the lower-frequency modes, the CH band positions can change both up- and downward, occasionally changing their ordering.

The relative band intensities are rather conserved under the environment variation. For camphor the ROA CH stretching region spectra were the most sensitive to the solvent variation as the change in solvent polarity causes sign flip for a band around 3070 cm^{-1}. For VCD, the signs do not change, but band positions and relative intensities do.

Frequencies, Functionals, and Basis Sets. Comparison of the harmonic frequencies obtained with different methods provides indication of their computational reliability. The Raman and ROA fenchone spectra and the error of average harmonic CH stretching frequencies calculated at 12 approximation levels are summarized in Figure 4. Clearly all the electronic methods significantly overestimate the CH stretching frequencies if compared to experiment, HF being the extreme case with an error of 260 cm^{-1}. On the other hand, compared to mPW2PLYP[30] as the most advanced and accurate approach, all the DFT methods provide the harmonic frequencies too low, obviously still with a large deviation (70−160 cm^{-1}) from experiment. This can only be improved by the PT2 and LVCI anharmonic corrections, included at the mPW2PLYP level, giving the average errors as 35 and 5 cm^{-1}, respectively.

Interestingly, the empirical dispersion correction,[30,63] designed to treat longer-range dispersion interactions inadequately described by some older DFT approaches,[64] had an ambiguous effect on the spectra. In comparison with the uncorrected computations, it made slightly worse the lowest (<~1200 cm^{-1}) and improved the higher-frequency region. The influence of the dispersion in the CH region is rather negligible (Figure 4).

More importantly, the performance of the harmonic level is much better for spectral shapes than for frequencies. As apparent from Figure 4, various functionals give similar intensity profiles, including the vibrational optical activity. Principal spectral features can thus be approximately modeled within the harmonic approach also for the CH stretching. As discussed previously, this approach can be combined, for example, with empirical scaling of the frequencies.[65,66]

The basis set convergence of the ROA and Raman spectra in the CH stretching and lower-frequency regions is analyzed in Figure 5. The normalized spectral overlap error comprises deviations of frequencies and intensities. Apparently, for the Raman and IR spectra, the convergence is reasonably smooth both for the CH and lower-frequency vibrations. The ROA and VCD spectra in the CH region (blue records in the panels) do not improve much with increasing basis set size before the 6-311++G** basis set is used. This indicates that the simulated VOA CH stretching spectra might be more sensitive not only to the proper inclusion of the solvent environment (see above), but also to the basis set. The split-valence triple-ζ 6-311++G** basis set brings an improvement mostly to the valence electrons determining vibrational frequencies; sole ROA intensities, for example, would be sufficiently described by the D95++** basis and similar sets including the diffuse functions.[27,39,67]

From a practical point of view, usage of basis sets larger than 6-311++G** thus appears unnecessary, as this is associated with a sharp increase of computational time. From Figure 5, we also see that for approximate computations a proper choice of the basis set can lead to significant time savings, because smaller basis sets sometime provide better results than larger ones. For convenience, we list the computational times needed for ROA spectra computation with different basis sets in Supporting Information Table S3.

For the following anharmonic modeling, we use the mPW2PLYP/6-311++G**/COSMO method for force field, which allows for both the harmonic and anharmonic force field term calculations in a reasonable time in a consistent way. Note that the B3LYP/6-311++G**/COSMO level is used for the intensities.

Comparison of the Anharmonic Approaches for α-Pinene. α-Pinene is the smallest of the three models and permissible for extended vibrational tests. The behavior of the harmonic, PT2, and LVCI computational method used for the spectral simulations is documented in Figure 6. All the Raman, ROA, IR, and VCD spectra are shown within 1350−1770 and 2700−3200 cm^{-1}, to capture the differences between the low-frequency and CH stretching regions. The indicated normal mode numbers correspond to Table 1. For LVCI, the normal mode number was assigned according to the dominant expansion coefficients.

The harmonic computation provides the CH stretching frequencies too high. Although the simulated harmonic spectral profiles are close to experiment, a band-to-band comparison at this level can be done only in the lower-frequency region. The PT2 computation corrects most of the frequency error.

dx.doi.org/10.1021/ct400285n | J. Chem. Theory Comput. XXXX, XXX, XXX−XXX

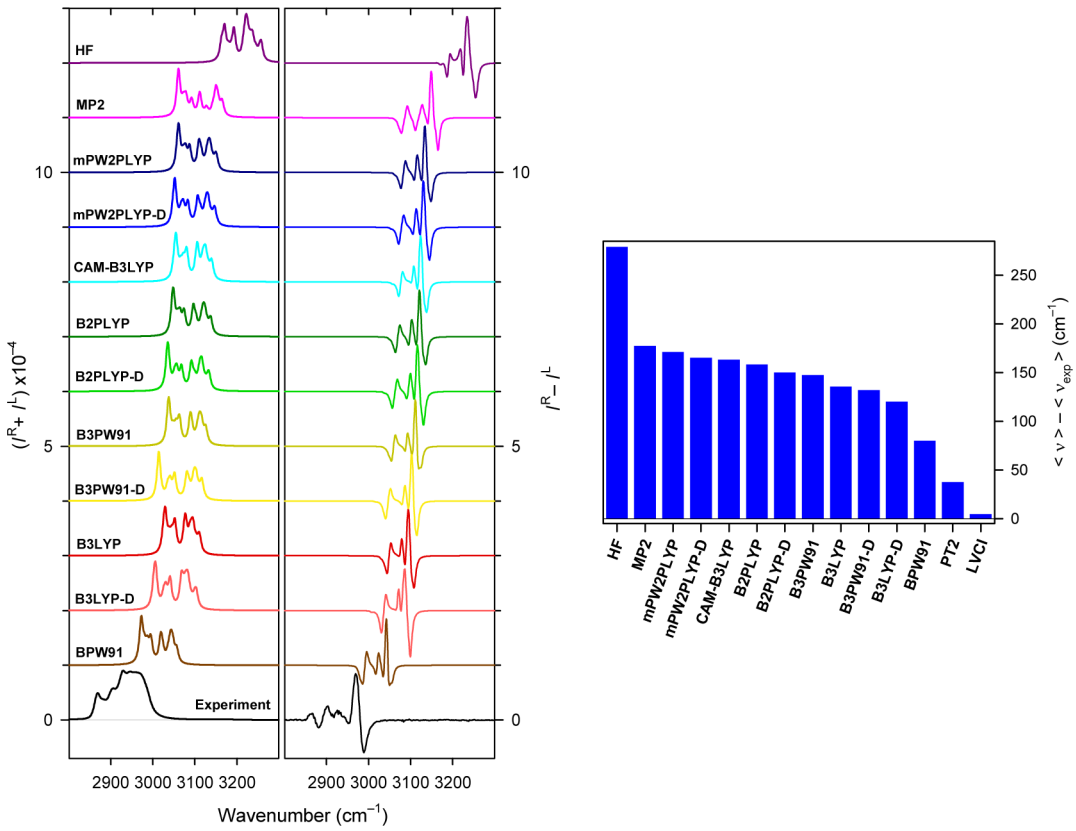

Figure 4. (left) Raman and ROA (1*R*)-(−)-fenchone spectra calculated by various harmonic methods, with the 6-311++G** basis set. (right) Average harmonic (HF...BPW91) and anharmonic (PT2 and LVCI, for the mPW2PLYP force field) frequency errors.

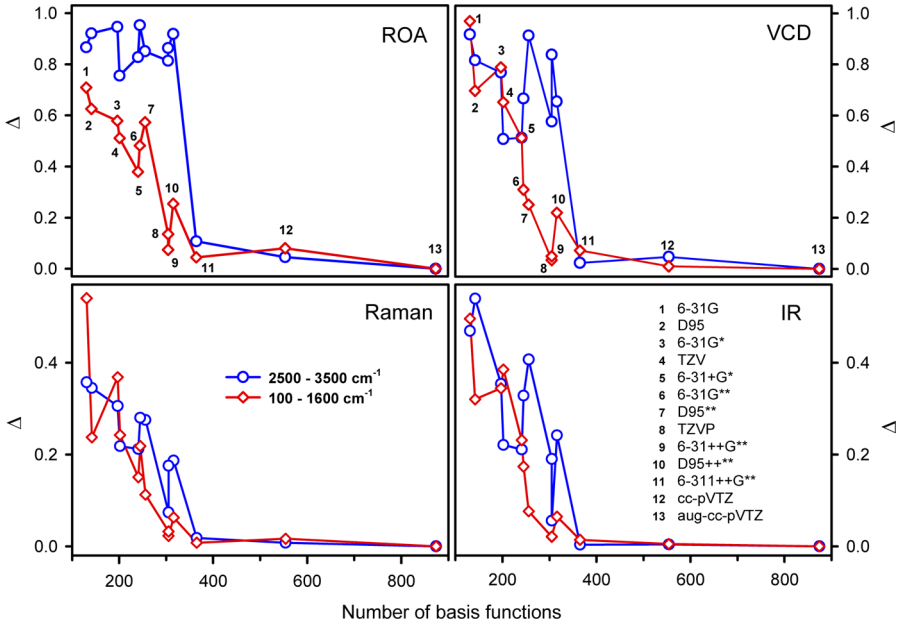

Figure 5. Basis set convergence of spectral errors, calculated for the four (1*R*)-(−)-fenchone spectral types using the B3LYP functional and aug-cc-pVTZ reference ($\Delta = 1 - |\int SS_{ref}\, d\nu| / [(\int S_{ref}^2\, d\nu)^{1/2} (\int S^2\, d\nu)^{1/2}]$.

To our surprise, the 1350−1770 cm^{-1} region also significantly benefited from the anharmonic computations. This wavenumber range comprises mostly the C−H bending modes, and is traditionally considered as harmonic. For example, mode number 24, shifted from the harmonic position at 1492 to 1418 cm^{-1}, is then only somewhat lower than experiment (1434 cm^{-1}). The C═C stretching band (mode number 17) is rather indifferent to anharmonicity corrections. Its position calculated too high if compared to experiment can be attributed most probably to an error of the mPW2PLYP/6-311++G**/COSMO force field. Possibly, also higher-order terms, not included in the potential (1) may play a role. Additionally, the LVCI

dx.doi.org/10.1021/ct400285n | *J. Chem. Theory Comput.* XXXX, XXX, XXX−XXX

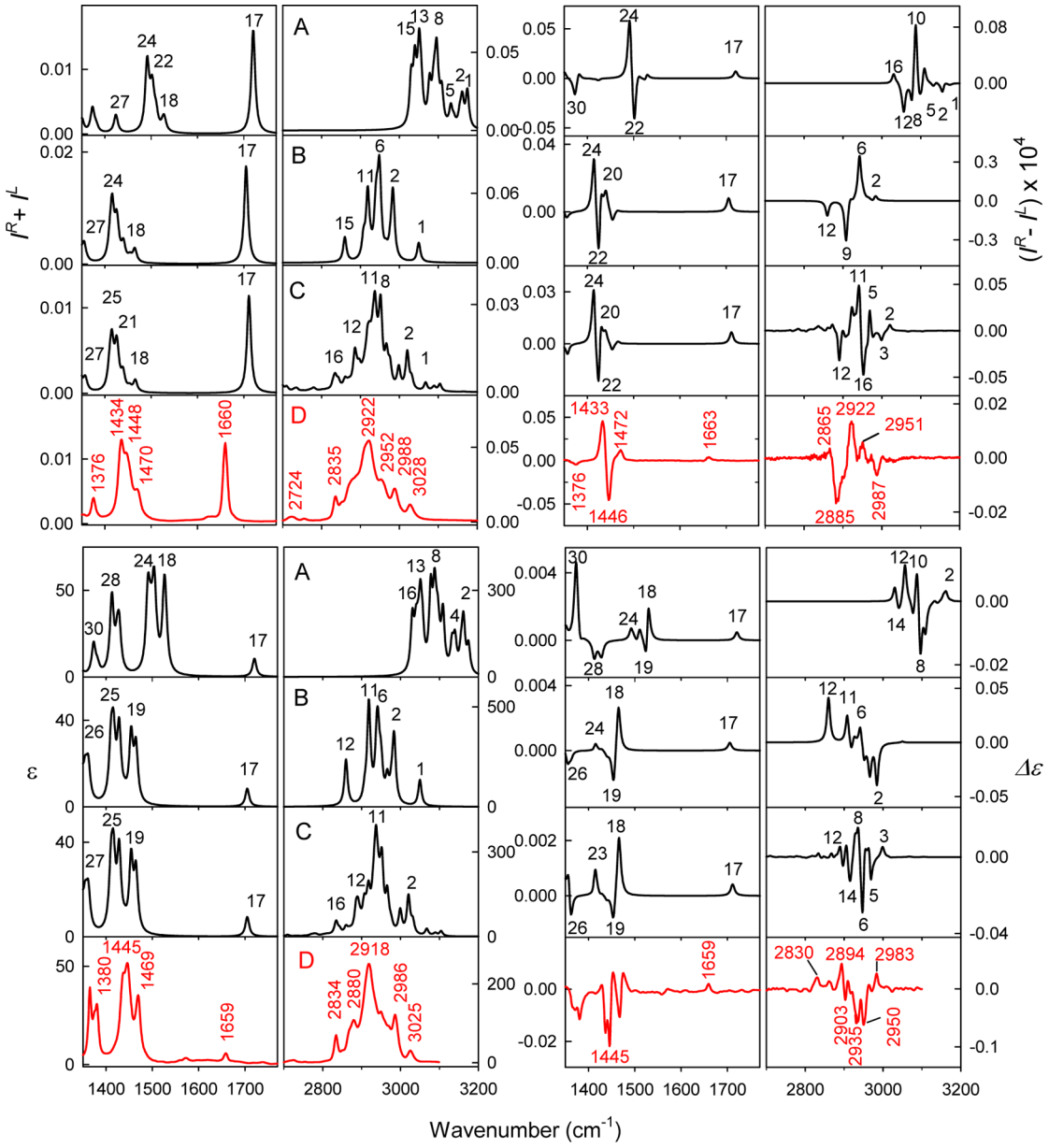

Figure 6. Raman, ROA, IR, and VCD spectra of (1*R*)-(+)-α-pinene calculated at the (A) harmonic, (B) PT2, and (C) LVCI (36 modes fixed, $c_1 = 0.002$, $c_2 = 0.1$, 749398 HO states) approximation levels and (D) experiment, in low (1350−1770 cm^{-1}) and CH (2700−3200 cm^{-1}) frequency regions. The indicated mode numbers correspond to Table 1.

computational method has been primarily optimized for the CH stretching region. In particular, the HO states potentially important for the C═C vibration could not be included in the Hamiltonian because of the size limits.

In the C−H stretching region the PT2 computation is still inadequate to reproduce the observed spectral shapes, although it improves the harmonic Raman and IR spectral shapes. The mode ordering is mostly conserved within PT2.

The LVCI computation is the most consistent with experiment, providing both reasonable frequencies and intensity profiles. This is visible namely for the Raman and IR spectra, where most simulated and experimental bands can be assigned also in the CH stretching region. In comparison with the harmonic profiles, the LVCI spectra become narrower and dominated by the central signal (vibration number 11, ∼2922 cm^{-1} for Raman). For ROA and VCD the intensity errors are more apparent than for IR and Raman scattering. This is given in general by the higher sensitivity of the polarized spectroscopies to molecular vibrations, i.e. to the eigenvectors of the LVCI Hamiltonian. Nevertheless, the simulation allows one to understand the underlying vibrational patterns. For ROA, for example (see also Figure 7, top, for detailed overlap of the simulation and experiment), the relatively strong negative signal observed at 2885 cm^{-1} is readily reproduced by LVCI at approximately the same position (with a strong participation of the fundamental mode number 12; note, however, that beyond the harmonic approximation the concept of vibrational normal modes becomes irrelevant). Similarly, the positive experimental band at 2922 cm^{-1} is reproduced by LVCI, with a participation of the normal mode 11. Around 2951 cm^{-1}, however, the negative LVCI ROA signal associated with the mode number 16 is overestimated by the computation.

For VCD, the behavior of the LVCI simulation is similar as for ROA, with the largest discrepancy around 2935 cm^{-1}, where a

dx.doi.org/10.1021/ct400285n | J. Chem. Theory Comput. XXXX, XXX, XXX−XXX

Table 1. Calculated (mPW2PLYP/6-311++G/COSMO) CH Stretching Normal Modes[a]**

mode	α-pinene		fenchone		camphor	
1	3175	1*	3150	3 ip 2 ip 3 ip 2	3158	3
2	3162	3 ip 2	3148	3 ip 2 op 3 ip 2	3141	3 ip 2
3	3156	3	3140	2 ip 2 ip 2 op 3 ip 3	3136	2 ip 2 ip 2
4	3140	3 op 2	3135	2 op 2 ip 2 op 3 ip 3	3135	3
5	3132	3	3132	3 op 3 op 2	3133	3
6	3109	3 ip 3	3131	3, 3 op 3	3130	2 op 2 ip 2
7	3102	3 op 3	3130	3, 3 op 3 op 2	3123	3 ip 3
8	3096	1 ip 1 ip 2	3130	3 op 2	3118	1, 2 op 2
9	3090	3	3118	1 ip 2, 2	3116	3 op 3
10	3087	1 op 1 ip 2	3115	1, 2 op 2	3113	1, 2 op 2
11	3078	1 op 2	3090	2 ip 2 ip 2 op 1	3090	1 op 2 ip 2 ip 2
12	3056	2*	3082	2 op 2 ip 2	3088	2 ip 2 op 2
13	3051	3 ip 3	3073	2 op 2	3080	2 op 2
14	3045	3 op 3	3062	3 ip 3	3063	3 ip 3 ip 3
15	3040	3	3059	3 op 3	3060	3 ip 3 op 3
16	3030	2* ip 1	3058	3	3056	3 op 3

[a]
1 - CH stretching
2 - asymmetric CH_2 stretching
2 - symmetric CH_2 stretching
3 - asymmetric CH_3 stretching
3 - symmetric CH_3 stretching
ip in phase
op out of phase
* proximate to double bond

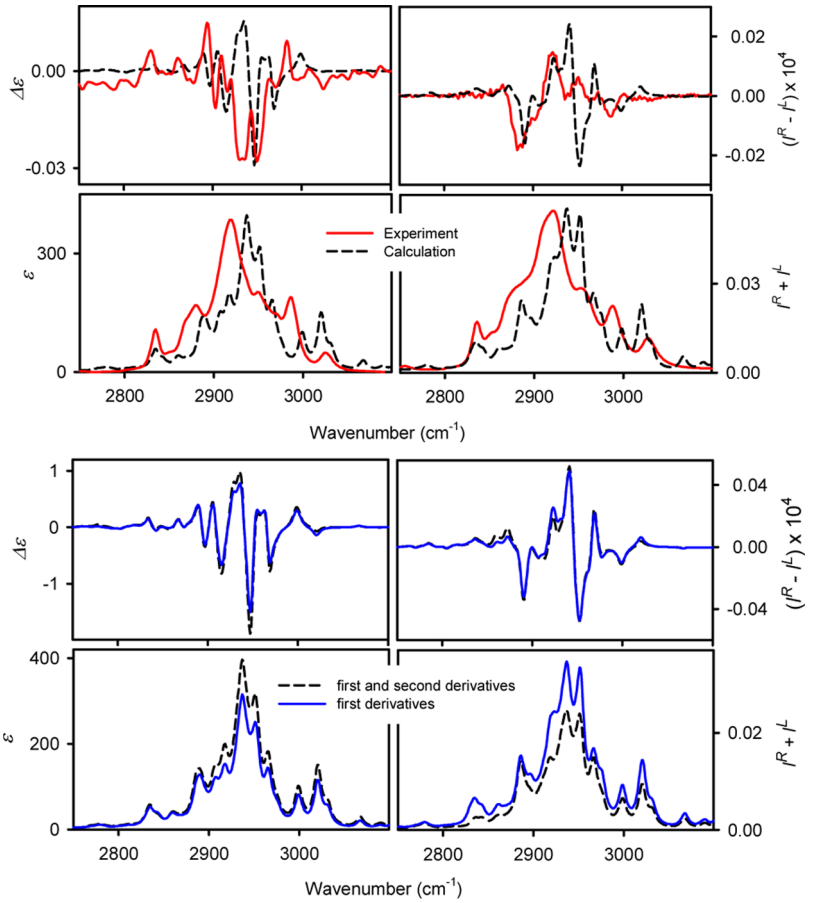

Figure 7. (top) Calculated (LVCI) and experimental VCD, IR, Raman, and ROA (1*R*)-(+)-*α*-pinene spectra in the CH stretching region. (bottom) Calculated spectra with and without contribution of the second intensity tensor derivatives.

negative signal is measured, but a positive one (mode number 8) is simulated. Overall, however, the convergence of the LVCI method to the experiment is quite apparent for all the spectral types. The simulation also justifies the above comparison of the harmonic ROA and VCD patterns to experiments, as even under LVCI some principal intensity profiles are conserved if compared to the harmonic limit. This suggests that the anharmonic interactions/potential shape only rarely causes changes in the mode ordering (e.g., via Fermi resonances). Instead, the CH stretching vibrations, for example, interact with a pool of other

dx.doi.org/10.1021/ct400285n | J. Chem. Theory Comput. XXXX, XXX, XXX−XXX

molecular vibrations, which causes an approximately uniform shift of the frequencies. There is a remaining frequency error of about 5−10 cm^{-1} of the LVCI computation, most probably given by the limited Taylor expansion of the potential, error of the electronic quantum-chemical approach, and approximation in the vibrational LVCI approach.

For IR and VCD the magnitude of the measured and computed intensities is directly comparable. For the absorption (Figure 6, left, bottom) all the computational models provide peak heights (for the bandwidth of 10 cm^{-1}) comparable with the experiment; the accuracy seems worse for the CH stretching region (where the calculated intensities are by about 30% overestimated) than below 1800 cm^{-1}. The anharmonic PT2 and LVCI anharmonic corrections do not seem to significantly change the harmonic integral IR intensities. The VCD intensities obtained with different models (Figure 6, right, bottom) vary more and a detailed qualitative comparison is problematic. On average, the harmonic VCD intensities appear underestimated (by ∼50%) if compared to experiment, which is significantly repaired by the anharmonic corrections.

The spectra simulated with and without the second derivatives of the intensity tensors (transitional electric and magnetic dipole moment, and the $\boldsymbol{\alpha}$, $\mathbf{G}'$, and $\mathbf{A}$ polarizabilities,[34] Figure 7, bottom) are very similar. Rather surprisingly, for the VOA intensities (VCD, ROA) generally considered very sensitive to computational parameters the contribution of the second derivatives is relatively smaller than for the IR and Raman spectra. Finally, we see that the second derivative contributions can both increase (IR) and decrease (Raman) the integral intensities. They mostly improve the agreement of the simulations with the experiment, and their computation requires relatively small computational effort in comparison with the energy derivatives.

Anharmonic Coupling Between Normal Modes and Convergence of the LVCI Results. The freezing of the lower-frequency vibrations is necessary to reduce the number of the HO states. Similar mode separation appeared useful, for example, in the modeling of the tryptophan chromophore.[68] It is based on the assumption of a limited coupling between the higher- and lower-frequency modes. At least partially, it can be justified on the basis of the anharmonic coupling defined as an average of the dimensionless cubic and quartic constants containing two modes i and j ($|c_{iii}| + |c_{jjj}| + |c_{iji}| + |d_{iiii}| + \ldots$). Indeed (Supporting Information Figure S4), the CH stretching modes (last 16 modes in the graphs) exhibit exceptionally large diagonal and off-diagonal anharmonic constants and are thus relatively isolated from other vibrations. The coupling of the CH stretching to the lower-frequency modes is significantly smaller, and even smaller is the diagonal and off-diagonal coupling within the modes with frequency below 2000 cm^{-1}. The coupling increases again for the very-low energy (<300 cm^{-1}, not shown) modes, such as the methyl torsions, where, however, the limited Taylor expansion of the potential (eq 1) is not applicable.

LVCI computations with a variable number of the HO states (with various coupling parameters c_1 and c_2 and number of blocked vibrations, e.g. Supporting Information Figure S5 with the Raman and ROA spectra of (1R)-(+)-α-pinene) indicate a good stability and convergence of the transition vibrational frequencies; however, the intensities are very sensitive and require a relatively large number of states to be included, especially for the one-step selection with $c_2 = 0$. This makes the computations extremely computer memory and time demanding.

On the other hand, the two-step HO basis set selection appears as a more reliable and accurate method. The role of the second parameter for the simulated Raman spectra of α-pinene is documented in Figure 8. If just states interacting with the CH

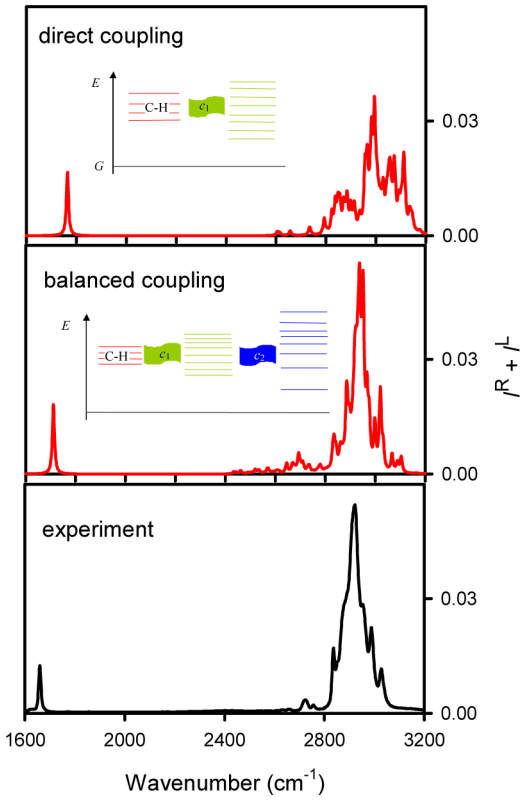

Figure 8. Raman spectra of α-pinene calculated by the LVCI method with one ($c_1 = 0.002$, $c_2 = \infty$) and two ($c_1 = 0.002$, $c_2 = 0.1$) step selection of the HO basis states and the experiment. The first method causes an unrealistic spread of state energies, whereas the second one provides more balanced coupling and spectra of the states of interest (CH stretching).

fundamental vibrations are selected, even for a relatively weak coupling ($c_1 = 0.002$), the resultant spectral shape is not very realistic, with a large dispersion of the CH stretching frequencies. The frequencies are also too high. This can be prevented by including the second set of states interacting with the first one, for $c_2 = 0.1$. Then the simulated frequencies and spectral shapes are significantly more realistic, albeit at the expense of the computer resources required (14 986 vs 749 398 states included). This approach leads to a more reliable convergence, where spectral intensities are less sensitive to the number of states included (see also Supporting Information Figures S5 and S6) than in the one step LVCI state selection.

On the basis of the perturbation formalism,[69] one may expect that adding a third set of states interacting with the two would further improve the data. This is not possible to explore for our systems (the total number of the states would be enormous) and implementation limited to 5-times excited states. On the other hand, from the large value of c_2 (0.1) we see that a significant improvement was already achieved by including the largest interactions, suggesting that further changes would bring minor effects only, with respect to all sources of errors. The possibility to vary the c_1 and c_2 coefficients arbitrarily makes the three-stage state selection obsolete as well.

dx.doi.org/10.1021/ct400285n | J. Chem. Theory Comput. XXXX, XXX, XXX−XXX

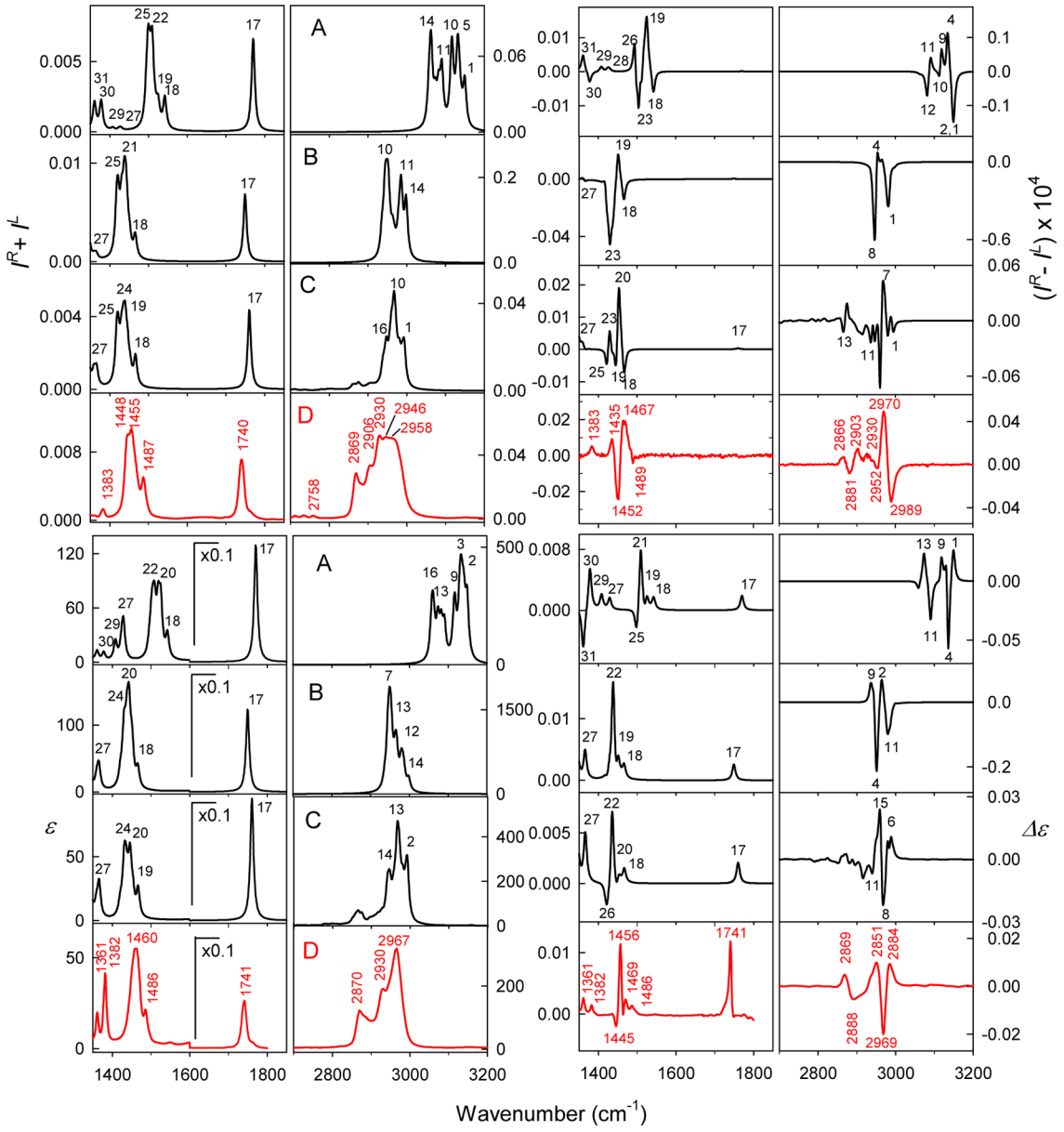

Figure 9. (1*R*)-(−)-Fenchone Raman, ROA, IR, and VCD spectra calculated at the (A) harmonic, (B) PT2, and (C) LVCI approximations (36 modes fixed, $c_1 = 0.002$, $c_2 = 0.1$, 1 086 008 HO states) and (D) experiment in low (1350−1850 cm^{-1}) and CH (2700−3200 cm^{-1}) frequency regions. The indicated mode numbers correspond to Table 1.

Fenchone and Camphor Spectra. The behavior of the other two molecules with respect to the spectral modeling of the CH stretching vibrations is similar to α-pinene (Figures 9 and 10, detailed overlaps between the calculation and experiment are plotted in Supporting Information Figure S7). The computations were slightly more demanding than for α-pinene because of the presence of the carbonyl group. For fenchone (Figure 9), the most visible discrepancies between the LVCI simulation and experiment are the shape of the Raman CH stretching signal, predicted to be sharper than observed, and the ROA band around 2989 cm^{-1}, the experimental negative sign of which is reproduced as a weak split signal only. At the level of visual comparison, a better agreement between the simulation and experiment is apparent for the IR and VCD spectra that for Raman/ROA.

For camphor (Figure 10), the intensity of the highest-frequency negative ROA signal at 2974 cm^{-1} is underestimated as well. In spite of structural similarity of camphor and fenchone, their spectra, in particular VCD and ROA, are rather different. For example, camphor ROA is much simpler than for fenchone, which is well reproduced by the LVCI computation, but not by the lower-level harmonic and PT2 approaches. For fenchone, the relative Raman and IR intensities of the C═O stretching band are smaller than for camphor, which is reproduced by all the computations.

The computational times can well be estimated for the electronic problem, where the harmonic force field is the most demanding part (for example, 188 h for camphor and the mPW2PLYP/6-311++G**/COSMO computation if recalculated to one E7330 2.40 GHz processor). Both the PT2 and LVCI methods need the same anharmonic force constants present in eq 1, which requires the time for the harmonic force field to be multiplied twice by the number of modes (resulting to the total of about 1175 CPU days in this case). Computational

dx.doi.org/10.1021/ct400285n | *J. Chem. Theory Comput.* XXXX, XXX, XXX−XXX

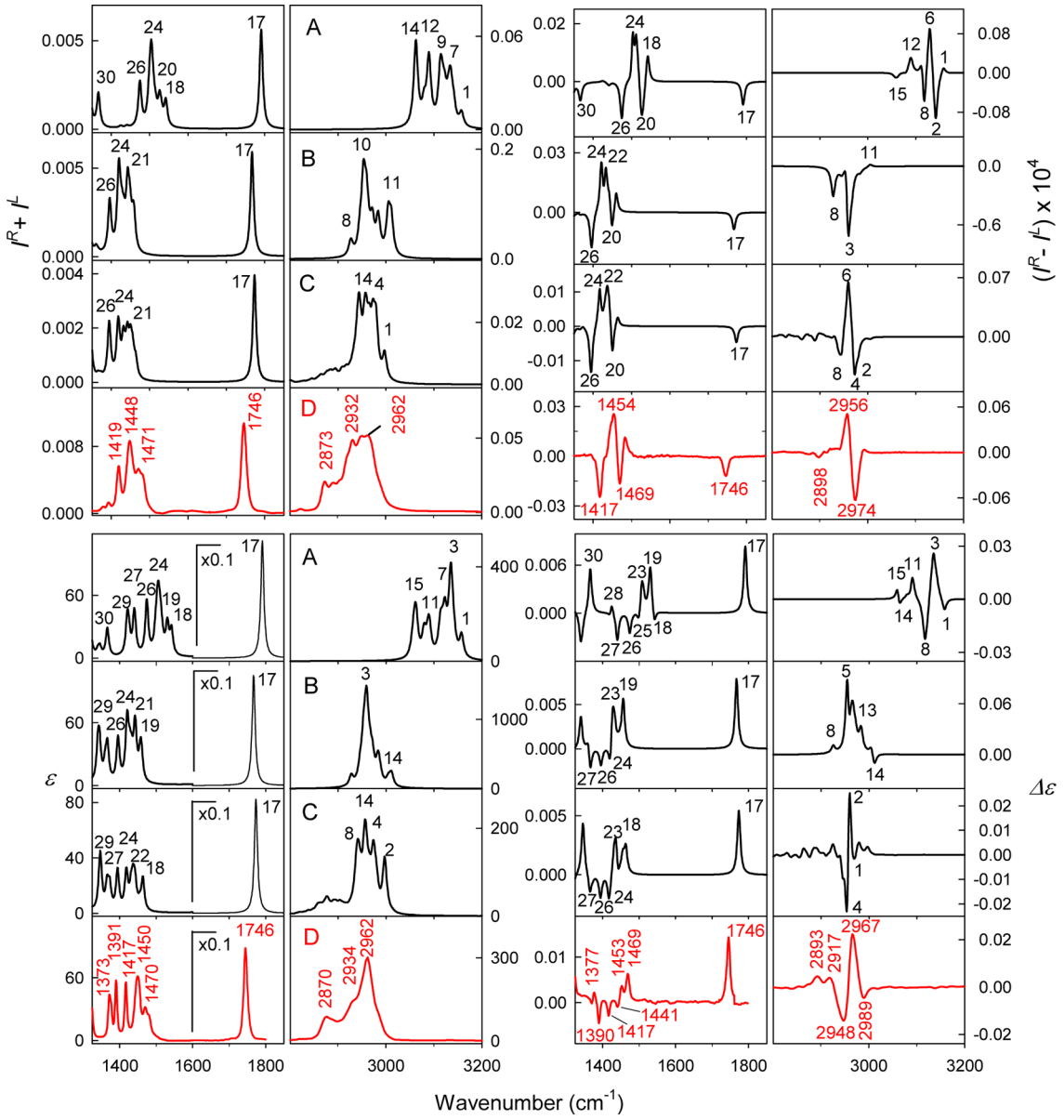

Figure 10. (1*R*)-(+)-Camphor Raman, ROA, IR, and VCD spectra calculated at the (A) harmonic, (B) PT2, and (C) LVCI approximations (31 modes fixed, $c_1 = 0.002$, $c_2 = 0.1$, 1 906 884 HO states) and (D) experiment in low (1350−1850 cm^{-1}) and CH (2800−3200 cm^{-1}) frequency regions. The indicated mode numbers correspond to Table 1.

times needed for the PT2 and LVCI vibrational procedures vary significantly. In our implementation, the PT2 correction took about 1 min and the LVCI camphor computation (Figure 10) took about 6 days.

In the spirit of the previous study of Cappelli et al. focused on the PT2 method,[26] we consider the possibility of reliable LVCI computations as a next step in reproduction of the CH stretching signal in organic molecules. This is clearly desirable as the harmonic approaches do not capture important spectral features and the link between the spectral shapes and structures. Apart of the dimensionality of the problem, many obstacles remain to be solved in the future, such as the role of the lowest-energy vibrations (e.g., methyl torsions), potentially requiring an explicit quantum state temperature averaging and extension of the limited Taylor expansion-based anharmonic approach.

CONCLUSIONS

We acquired high-quality ROA spectra of three terpene molecules, and by comparing the four spectral types with computations, we could assess performance of the computational approaches for detailed CH stretching modeling. Contrary to general belief, we found that the CH stretching spectral intensities are very dependent on the solvent environment and are also slightly more sensitive to the basis set choice than the lower-frequency vibrations.

For the simulation beyond the harmonic limit, a limited interaction between the CH stretching and lower-frequency modes was assumed. This could be partially justified by analysis of the anharmonic intermode coupling. Owing to an efficient implementation of the diagonalization procedure, the limited vibrational configuration interaction provided converged spectral patterns very well reproducing the experimental frequencies and intensities. In spite of occasional problems namely for the

dx.doi.org/10.1021/ct400285n | *J. Chem. Theory Comput.* XXXX, XXX, XXX−XXX

vibrational optical activity spectral features, the LVCI scheme appears as the best simulation method so far, over performing the harmonic and second-order perturbational approaches. The computations in part justify previous modeling efforts based on the harmonic limit, as the most distinct spectral features survive also beyond the harmonic approximation. A future accuracy improvement is desirable; nevertheless the results clearly indicate that the LVCI simulation of the vibrational optical activity beyond the harmonic limit are possible and bring precious information about molecular structure and the spectroscopic response.

■ ASSOCIATED CONTENT

Supporting Information

Experimental and computational details including all experimental spectra and solvent dependence of the calculated results. This material is available free of charge via the Internet at http://pubs.acs.org.

■ AUTHOR INFORMATION

Corresponding Author

*E-mail: bour@uochb.cas.cz.

Notes

The authors declare no competing financial interest.

■ ACKNOWLEDGMENTS

This study was performed with the support from the Academy of Sciences (M200550902), Grant Agency of the Czech Republic (P208/11/0105), Grant Agency of Charles University (126310), and the Ministry of Education (LH11033).

■ REFERENCES

(1) Hug, W.; Haesler, J. *Int. J. Quantum Chem.* **2005**, *104*, 695−715.
(2) Zuk, W. M.; Freedman, T. B.; Nafie, L. A. *Biopolymers* **1989**, *28*, 2025−2044.
(3) Julínek, O.; Lindner, W.; Urbanová, M. *Chirality* **2011**, *23*, 354−360.
(4) Debie, E.; Jaspers, L.; Bultinck, P.; Herrebout, W.; Veken, B. V. D. *Chem. Phys. Lett.* **2008**, *450*, 426−430.
(5) Guo, C.; Shah, R. D.; Mills, J.; Dukor, R. K.; Cao, X.; Freedman, T. B.; Nafie, L. *Chirality* **2006**, *18*, 775−782.
(6) Keiderling, T. A.; Kubelka, J.; Hilario, J., Vibrational circular dichroism of biopolymers. Summary of methods and applications. In *Vibrational spectroscopy of polymers and biological systems*; Braiman, M., Gregoriou, V., Eds.; CRC Press: Boca Raton, 2006; pp 253−324.
(7) Nafie, L. *Vibrational optical activity: Principles and applications*; Wiley: Chichester, 2011.
(8) Benda, L.; Štěpánek, J.; Kaminský, J.; Bouř, P. Spectroscopic Analysis: Ab initio Calculation of Chiroptical Spectra. In *Comprehensive Chirality*; Carreira, E. M., Yamamoto, H., Eds.; Elsevier: Amsterdam, 2012; Vol. *8*, pp 520−544.
(9) Polavarapu, P. L.; Nafie, L. *J. Chem. Phys.* **1980**, *73*, 1567−1575.
(10) Longhi, G.; Abbate, S.; Gangemi, R.; Giorgio, E.; Rosini, C. *J. Phys. Chem. A* **2006**, *110*, 4958−4968.
(11) Guo, C.; Shah, R. D.; Dukor, R. K.; Freedman, T. B.; Cao, X.; Nafie, L. A. *Vib. Spectrosc.* **2006**, *42*, 254−272.
(12) Bounouar, M.; Scheurer, C. *Chem. Phys.* **2006**, *323*, 87−101.
(13) Parchaňský, V.; Bouř, P. *J. Chem. Phys.* **2010**, *133*, 044117.
(14) Daněček, P.; Kapitán, J.; Baumruk, V.; Bednárová, L.; Kopecký, V., Jr.; Bouř, P. *J. Chem. Phys.* **2007**, *126*, 224513.
(15) Daněček, P.; Bouř, P. *J. Comput. Chem.* **2007**, *28*, 1617−1624.
(16) Bouř, P. *J. Phys. Chem.* **1994**, *98*, 8862−8865.
(17) Kaledin, A. L.; Bowman, J. M. *J. Phys. Chem. A* **2007**, *111*, 5593−5598.
(18) Romanowski, H.; Bowman, J. M.; Harding, L. B. *J. Chem. Phys.* **1985**, *82*, 4155−4165.
(19) Laux, L.; Pultz, V.; Abbate, S.; Havel, H. A.; Overend, J.; Moscowitz, A. *J. Am. Chem. Soc.* **1982**, *104*, 4276−4278.
(20) Devlin, F. J.; Stephens, P. J.; Cheeseman, J. R.; Frisch, M. J. *J. Phys. Chem.* **1997**, *101*, 9912−9924.
(21) Samsonyuk, A.; Scheurer, C. *J. Comput. Chem.* **2013**, *34*, 27−37.
(22) Choi, J. H.; Cho, M. *J. Chem. Theory Comput.* **2011**, *7*, 4097−4103.
(23) Hanson-Heine, M. W. D.; George, M. W.; Besley, N. A. *J. Chem. Phys.* **2012**, *136*, 224102.
(24) Carbonniere, P.; Lucca, T.; Pouchan, C.; Rega, N.; Barone, V. *J. Comput. Chem.* **2005**, *26*, 384−388.
(25) Polyanichko, A. M.; Andrushchenko, V.; Bouř, P.; Wieser, H., Vibrational Circular Dichroism Studies of Biological Macromolecules and their Complexes. In *Circular Dichroism: Theory and Spectroscopy*; Rodgers, D. S., Ed.; Nova: Hauppauge, NY, 2011.
(26) Cappelli, C.; Bloino, J.; Lipparini, F.; Barone, V. *J. Phys. Chem. Lett.* **2012**, *3*, 1766−1773.
(27) Cheeseman, J. R.; Frisch, M. J. *J. Chem. Theory Comput.* **2011**, *7*, 3323−3334.
(28) Barone, V. *J. Chem. Phys.* **2005**, *122*, 014108.
(29) Ivani, I.; Bouř, P. *J. Chem. Theory Comput.* **2010**, *6*, 2095−2102.
(30) Schwabe, T.; Grimme, S. *Phys. Chem. Chem. Phys.* **2007**, *9*, 3397−3406.
(31) Møller, C.; Plesset, M. S. *Phys. Rev.* **1934**, *46*, 618−622.
(32) Parr, R. G.; Yang, W. *Density-functional theory of atoms and molecules*; Oxford University Press: New York, 1994.
(33) Hanzlíková, J.; Praus, P.; Baumruk, V. *J. Mol. Struct.* **1999**, *480−481*, 431−435.
(34) Barron, L. D. *Molecular Light Scattering and Optical Activity*; Cambridge University Press: Cambridge, 2004.
(35) Frisch, M. J.; Trucks, G. W.; Schlegel, H. B.; Scuseria, G. E.; Robb, M. A.; Cheeseman, J. R.; Scalmani, G.; Barone, V.; Mennucci, B.; Petersson, G. A.; Nakatsuji, H.; Caricato, M.; Li, X.; Hratchian, H. P.; Izmaylov, A. F.; Bloino, J.; Zheng, G.; Sonnenberg, J. L.; Hada, M.; Ehara, M.; Toyota, K.; Fukuda, R.; Hasegawa, J.; Ishida, M.; Nakajima, T.; Honda, Y.; Kitao, O.; Nakai, H.; Vreven, T.; Montgomery, J., J. A.; Peralta, J. E.; Ogliaro, F.; Bearpark, M.; Heyd, J. J.; Brothers, E.; Kudin, K. N.; Staroverov, V. N.; Kobayashi, R.; Normand, J.; Raghavachari, K.; Rendell, A.; Burant, J. C.; Iyengar, S. S.; Tomasi, J.; Cossi, M.; Rega, N.; Millam, J. M.; Klene, M.; Knox, J. E.; Cross, J. B.; Bakken, V.; Adamo, C.; Jaramillo, J.; Gomperts, R.; Stratmann, R. E.; Yazyev, O.; Austin, A. J.; Cammi, R.; Pomelli, C.; Ochterski, J. W.; Martin, R. L.; Morokuma, K.; Zakrzewski, V. G.; Voth, G. A.; Salvador, P.; Dannenberg, J. J.; Dapprich, S.; Daniels, A. D.; Farkas, O.; Foresman, J. B.; Ortiz, J. V.; Cioslowski, J.; Fox, D. J. *Gaussian 09*, Revision B01, Gaussian, Inc.: Wallingford CT, 2009.
(36) Perdew, J. P.; Burke, K.; Wang, Y. *Phys. Rev. B* **1996**, *54*, 16533−16539.
(37) Yanai, T.; Tew, D.; Handy, N. C. *Chem. Phys. Lett.* **2004**, *393*, 51−57.
(38) Grimme, S. *J. Comput. Chem.* **2006**, *27*, 1787−1799.
(39) Zuber, G.; Hug, W. *J. Phys. Chem. A* **2004**, *108*, 2108−2118.
(40) Ruud, K.; Helgaker, T.; Bouř, P. *J. Phys. Chem. A* **2002**, *106*, 7448−7455.
(41) Ruud, K.; Thorvaldsen, J. *Chirality* **2009**, *21*, E54−E67.
(42) Klamt, A. COSMO and COSMO-RS. In *The Encyclopedia of Computational Chemistry*; Schleyer, P. R., Allinger, N. L., Clark, T., Gasteiger, J., Kollman, P. A., Schaefer, H. F., III, Schreiner, P. R., Eds.; John Wiley & Sons: Chichester, 1998; Vol. *1*, pp 604−615.
(43) Buckingham, A. D. *Proc. R. Soc. (London) A* **1956**, *238*, 235−244.
(44) Polavarapu, P. L. *Vibrational spectra: principles and applications with emphasis on optical activity*; Elsevier: Amsterdam, 1998; Vol. *85*.
(45) Papoušek, D.; Aliev, M. R. *Molecular Vibrational/Rotational Spectra*; Academia: Prague, 1982.
(46) Dračínský, M.; Bouř, P. *J. Comput. Chem.* **2012**, *33*, 1080−1089.
(47) Stephens, P. J. *J. Phys. Chem.* **1985**, *89*, 748−752.
(48) Polavarapu, P. L. *Vibr. Spectra Struct.* **1984**, *13*, 103−160.

(49) Mitin, A. V. *J. Comput. Chem.* **1994**, *15*, 747−751.
(50) Davidson, E. R. *J. Comput. Phys.* **1975**, *17*, 87−94.
(51) Hug, W.; Kint, S.; Bailey, G. F.; Schere, J. R. *J. Am. Chem. Soc.* **1975**, 97.
(52) Hecht, L.; Che, D.; Nafie, L. A. *J. Phys. Chem.* **1992**, *96*, 4266−4270.
(53) Bouř, P.; McCann, J.; Wieser, H. *J. Phys. Chem. A* **1998**, *102*, 102−110.
(54) Bouř, P.; Baumruk, V.; Hanzlíková, J. *Collect. Czech. Chem. Commun.* **1997**, *62*, 1384−1395.
(55) Devlin, F. J.; Stephens, P. J.; Cheeseman, J. R.; Frisch, M. R. *J. Am. Chem. Soc.* **1996**, *118*, 6327−6328.
(56) Hug, W. *Appl. Spectrosc.* **1981**, *35*, 115−124.
(57) Haesler, J.; Schindelholz, I.; Riguet, E.; Bochet, C. G.; Hug, W. *Nature* **2007**, *446*, 526−529.
(58) Luber, S.; Reiher, M. *J. Phys. Chem. B* **2010**, *114*, 1057−1063.
(59) Kubelka, J.; Keiderling, T. A. *J. Phys. Chem. A* **2001**, *105*, 10922−10928.
(60) Bouř, P.; Keiderling, T. A. *J. Phys. Chem. B* **2005**, *109*, 23687−23697.
(61) Kubelka, J.; Huang, R.; Keiderling, T. A. *J. Phys. Chem. B* **2005**, *109*, 8231−8243.
(62) Ganim, Z.; Chung, H. S.; Smith, A. W.; Deflores, L. P.; Jones, K. C.; Tokmakoff, A. *Acc. Chem. Res.* **2008**, *41*, 432−441.
(63) Grimme, S.; Antony, J.; Ehrlich, S.; Krieg, H. *J. Chem. Phys.* **2010**, *132*, 154104.
(64) Šponer, J.; Hobza, P. *Collect. Czech. Chem. Commun.* **2003**, *68*, 2231−2282.
(65) Scott, A. P.; Radom, L. *J. Phys. Chem.* **1996**, *100*, 16502−16513.
(66) Merrick, J. P.; Moran, D.; Radom, L. *J. Phys. Chem. A* **2007**, *111*, 11683−11700.
(67) Reiher, M.; Liegeois, V.; Ruud, K. *J. Phys. Chem. A* **2005**, *109*, 7567−7574.
(68) Kabeláč, M.; Hobza, P.; Špirko, V. *Phys. Chem. Chem. Phys.* **2009**, *11*, 3921−3926.
(69) Szabo, A.; Ostlund, N. S. *Modern quantum chemistry. Introduction to advanced electronic structure theory*; Dover: New York, 1989.